nature structural & molecular biology

Evidence for a group II intron–like catalytic triplex in the spliceosome

Sebastian M Fica[1,2,7], Melissa A Mefford[3,6,7], Joseph A Piccirilli[4,5] & Jonathan P Staley[2]

To catalyze pre-mRNA splicing, U6 small nuclear RNA positions two metals that interact directly with the scissile phosphates. U6 metal ligands correspond stereospecifically to metal ligands within the catalytic domain V of a group II self-splicing intron. Domain V ligands are organized by base-triple interactions, which also juxtapose the 3′ splice site with the catalytic metals. However, in the spliceosome, the mechanism for organizing catalytic metals and recruiting the substrate has remained unclear. Here we show by genetics, cross-linking and biochemistry in yeast that analogous triples form in U6 and promote catalytic-metal binding and both chemical steps of splicing. Because the triples include an element that defines the 5′ splice site, they also provide a mechanism for juxtaposing the pre-mRNA substrate with the catalytic metals. Our data indicate that U6 adopts a group II intron–like tertiary conformation to catalyze splicing.

Introns are removed from pre-mRNAs by the spliceosome—a dynamic ribonucleoprotein machine composed of 80 conserved proteins and five small nuclear RNAs (snRNAs)[1]. Although proteins have key supporting roles in catalysis[2,3], the catalytic core itself is composed of RNA[4]. Indeed, this RNA-based core catalyzes two sequential phosphotransesterifications that are identical to the reactions performed by group II intron RNAs, which self-splice in the absence of proteins. Specifically, in both systems an intronic 2′-hydroxyl first attacks the 5′ splice site to form a branched lariat structure[5], and then the 5′ exon attacks the 3′ splice site to form mRNA. These two reactions were proposed to be catalyzed by a general two-metal mechanism[6], in which one divalent metal stabilizes the nucleophile, and the second divalent metal stabilizes the leaving group. Indeed, crystal structures of group II introns have revealed that ligands in the catalytic domain V position two divalent metals within 4 Å, the preferred distance for the two-metal mechanism, and that these metals interact with the 5′ splice site[7–10]. Supporting a catalytic role for these metals, divalent metals stabilize the leaving groups during group II intron splicing, thus promoting catalysis[9,10]. Indicating a two-metal mechanism for pre-mRNA splicing as well, we have recently demonstrated that ligands in U6 snRNA (**Fig. 1a**) bind two distinct divalent metals that catalyze splicing by interacting with the leaving groups during both chemical steps[4].

In the group II intron catalytic core, the conserved AGC triad of domain V together with nucleotides in the upper portion of the stem-loop, including a conserved bulged position, bind two distinct metals[7,11] (**Fig. 1b**,c). The ligands that form the two metal sites are brought together by base-triple interactions between the AGC triad and the bulge in a configuration stabilized by a conserved distal element termed the J2/3 linker[12,13] (**Fig. 1b**,**c**). By organizing domain V, the triple helix positions the two catalytic metals with the 4-Å spacing preferred for phosphoryl transfer catalysis[6,8,10]. Additionally, the J2/3 linker functions in both steps of splicing[12,13] and recognizes the 3′ splice site[14], thereby promoting docking of the 3′ splice site into the catalytic core. Thus, in the group II intron the triple helix effects catalysis both by positioning catalytic-metal ligands and by recruiting the 3′ splice site. In the spliceosome, however, the mechanism for catalytic-metal positioning and substrate docking has remained unclear.

Nonetheless, the RNA structures at the heart of the spliceosome share several similarities to the catalytic core of group II introns. Like RNA domains of group II introns, the snRNAs define and juxtapose the chemically reactive sites in the substrate, through U2–U6 helix Ia and adjacent interactions[15–17] (**Fig. 1a**). Additionally, similarly to the catalytic domain V of group II introns, U2–U6 helix Ib and the intramolecular stem-loop (ISL) of U6 adopt a secondary structure in which a conserved AGC triad is situated 5 bp away from a conserved bulge (**Fig. 1a**,**b**); both the triad and the bulge are important for each step in splicing[15,17–20]. Moreover, the U6 catalytic-metal ligands, situated in the triad and the bulge, correspond directly and stereospecifically to the domain V metal ligands[4,7,8].

The functional and structural similarities between group II introns and the spliceosome led to the prediction that a group II–like triple helix may form in U6 snRNA to similarly position analogous metal ligands. This spliceosomal triplex would join the AGC triad, the bulge and the terminal GA of the conserved ACAGAGA sequence[11] (**Fig. 1a**). Because the 5′ end of the ACAGAGA sequence base-pairs with the 5′ splice site[21,22], such a triple helix would also provide a structural

[1]Graduate Program in Cell and Molecular Biology, University of Chicago, Chicago, Illinois, USA. [2]Department of Molecular Genetics and Cell Biology, University of Chicago, Chicago, Illinois, USA. [3]Committee on Genetics Genomics and Systems Biology, University of Chicago, Chicago, Illinois, USA. [4]Department of Chemistry, University of Chicago, Chicago, Illinois, USA. [5]Department of Biochemistry and Molecular Biology, University of Chicago, Chicago, Illinois, USA. [6]Present address: Department of Biology, Johns Hopkins University, Baltimore, Maryland, USA. [7]These authors contributed equally to this work. Correspondence should be addressed to J.P.S. (jstaley@uchicago.edu).

Received 19 December 2013; accepted 27 March 2014; published online 20 April 2014; doi:10.1038/nsmb.2815

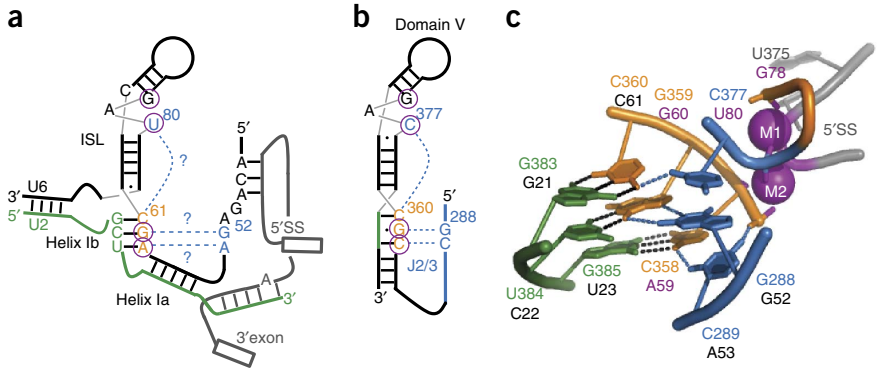

Figure 1 Base-triple interactions in the group II intron catalytic core and their proposed counterparts in the spliceosome. (**a**,**b**) Secondary-structure model of key RNA structures present in the spliceosomal (**a**) and group II intron (**b**) catalytic cores. Orange, residues in the catalytic triad; green, their base-pairing partners; blue, residues involved in base-triple interactions in domain V and their proposed counterparts in U6; circles, U6 and domain V residues that bind catalytic metals[4,7]; blue dashed lines with question marks, base-triple interactions tested in this study. The pre-mRNA in **a** is shown in gray in a configuration before branching. (**c**) Structure of the group II intron domain V, highlighting the catalytic triplex (PDB 4FAQ[8]). Coloring is as in **a**. Residue numbers are shown in orange, green and blue for the group II intron, with the proposed corresponding residues in the U6 snRNA denoted below in black or magenta (for catalytic-metal ligands). Black dashed lines, Watson–Crick interactions; blue dashed lines, base-triple interactions. The catalytic metals (M1 and M2), their nonbridging oxygen ligands and the scissile phosphate at the 5′ splice site are colored magenta. This particular class of group II introns contains an unusual CGC triad rather than the canonical AGC.

mechanism for docking of the 5′ splice site into the catalytic RNA core, a process required for both transesterifications. Recently, three-dimensional modeling of the spliceosomal active site revealed that such a triplex is consistent with current experimental data[23]. To determine whether the U6 snRNA positions catalytic metals in a manner similar to that of domain V of group II introns, we therefore investigated whether a group II intron–like catalytic triplex forms in the U6 snRNA.

Through molecular genetics *in vivo* and *in vitro*, in combination with site-directed cross-linking, we present evidence that a triple helix equivalent to that seen in domain V forms in U6 snRNA during catalytic activation of the spliceosome. Our data define a structural mechanism by which the spliceosome positions two metals in a catalytic configuration and juxtaposes these metals with the substrate reactive groups within a single catalytic core for both steps of splicing.

RESULTS

Genetic evidence for the U6 triplex

The AGC triad of U6 snRNA can base-pair with U6 downstream, to form an extended ISL[16,24]; with U4, to form U4–U6 stem I[25]; and with U2, to form U2–U6 helix Ib[15,19]. However, genetics implicates a function for the AGC triad beyond these roles[15,19]. For instance, a thorough *in vivo* compensatory analysis that repaired all of these predicted base-pairing interactions was unable to alleviate the lethality of three mutations in the AGC triad[19]. To determine whether the residual function of the AGC triad reflects formation of a catalytic triplex (**Fig. 1**), we exhaustively tested whether the growth defects of the AGC triad could be suppressed in an allele- and position-specific manner by compensatory mutations in the predicted base-triple partners[7,8,11] (**Supplementary Note 1**). A similar mutational approach has been applied previously in the study of triple-helix interactions in other RNAs[26,27] and subsequently validated by direct structural observation with NMR or X-ray crystallography[27,28].

The final position of the AGC triad, C61 of U6, has been predicted to interact with the bulged U6 ISL residue U80, which binds two catalytic metals[4,7,11] (**Fig. 1a**). Whereas C61 is tolerant to mutation[15,19], the C61G mutation grows slowly, even when helix Ib is repaired by a compensatory mutation in U2 (ref. 19; **Fig. 2**), thus allowing us to assay for suppression by U6 U80 mutations. Strikingly, U80C suppressed the growth defect of this repaired helix Ib double mutant (**Fig. 2a**). Suppression was specific with respect to both allele and position; other alleles at U80 did not improve growth of the helix Ib double mutant (**Fig. 2a**), and U80C did not suppress the growth defect of mutations at other positions in the AGC triad, such as A59U or G60U (**Fig. 2b** and **Supplementary Fig. 1a**), which were by contrast suppressed by mutations in their respective predicted base-triple partners (described below). Indeed, U80C exacerbated mutations at A59 and G60 (**Fig. 2b** and **Supplementary Table 1**), a result that would be expected for simultaneous disruption of two different base-triple interactions within a triple helix, as observed for the PAN RNA triplex[27]. Thus, the specific suppression by U80C provides evidence for a direct interaction between the bulged U80 in the U6 ISL and U6 C61 of the AGC triad (**Supplementary Note 2**).

The other two positions of the AGC triad, G60 and A59 of U6, have been predicted to pair with G52 and A53 of U6, respectively, from the conserved ACAGAGA sequence. Importantly, these two residues

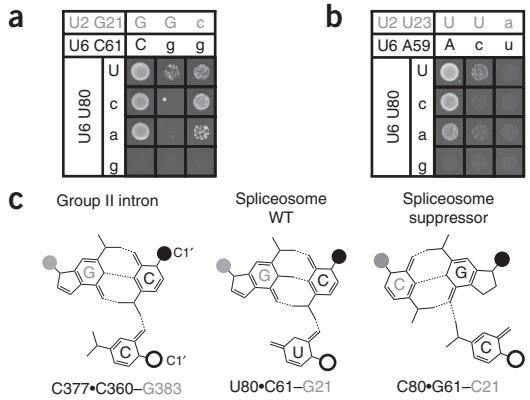

Figure 2 Genetic evidence for a base-triple interaction between U80 and C61 in the U6 snRNA. (**a**,**b**) Spot assays showing growth on selective medium of equivalent numbers of yeast cells containing combinations of alleles at U80 and either C61 (**a**) or A59 (**b**) of U6. The allele combinations for the U2–U6 helix Ib base pair mutated in each case are indicated above each panel. Alleles of U6 U80 present in each row are indicated on the left. (**c**) Diagrams of isomorphic base-triple interactions: C•C-G (left, as in group II intron structure[11]), U•C-G (middle, predicted for the spliceosome) and C•G-C (right, predicted for the spliceosome suppressor). The location of the glycosyl bond is highlighted with a circle: open black, major groove–interacting residue; filled black, catalytic triad; gray, U2 or equivalent residues in group II intron. WT, wild type. Uppercase represents wild-type allele; lowercase represents mutant allele.

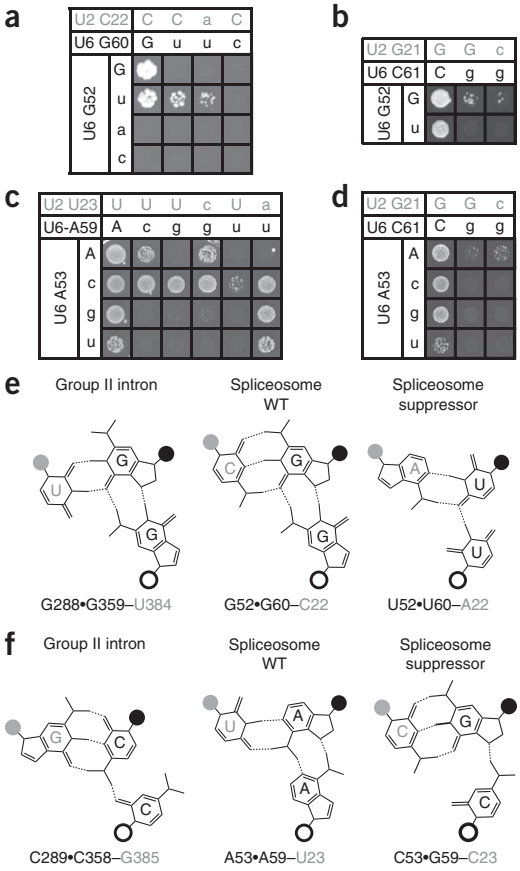

Figure 3 Genetic evidence for base-triple interactions between the AGC triad and the ACAGAGA 5′ splice site–binding region of the U6 snRNA. (**a**,**b**) Spot assays showing growth on selective medium of equivalent numbers of yeast cells containing combinations of alleles at G52 and either G60 (**a**) or C61 (**b**). (**c**,**d**) Spot assays showing growth on selective medium of equivalent numbers of yeast cells containing combinations of alleles at A53 and either A59 (**c**) or C61 (**d**). Matrices are presented as in **Figure 2a**,**b**. In **a**, yeast also contained a mutation at position 59 in U4 to repair U4–U6 stem I[19]. Additional positional-specificity controls are in **Supplementary Figure 1**. (**e**,**f**) Diagrams of observed (group II intron) and predicted (spliceosome) isomorphic base-triple interactions[11] involving the first (**f**) and second (**e**) residues of the catalytic triad. Diagrams are as in **Figure 2c**.

fall between the 5′ splice site–binding site of U6 and U2–U6 helix Ia, the latter of which is immediately adjacent to the catalytic core, such that triplex formation would promote docking of the 5′ splice site into the catalytic core[11] (**Fig. 1a**). All three point mutations at the central position of the AGC triad, G60, are lethal, and only the conservative substitution G60A can be suppressed by restoring base-pairing in U2–U6 helix Ib[15,19]. Nevertheless, we found that a mutation of the predicted base-triple residue, G52, suppressed G60U, albeit mildly (**Fig. 3a**). To our knowledge, this marks the first observed suppression of G60U (**Supplementary Note 3**). Remarkably, suppression of G60U did not require restoration of base-pairing in U2–U6 helix Ib (**Fig. 3a**). As we observed for mutations at U6 C61 (**Fig. 2**), suppression of G60U was specific with respect to allele and position (**Fig. 3a**,**b**, **Supplementary Fig. 1b** and **Supplementary Note 4**), thus providing compelling evidence for an interaction between G52 of the ACAGAGA sequence and G60 of the AGC triad, in the context of a base triple that includes helix Ib base-pairing.

Mutations at U6 A59 showed a wider range of phenotypes, thus allowing for multiple tests of suppression at this position. Although restoration of U2–U6 helix Ib suppresses A59C and A59G almost completely, A59U is not suppressed at all by restoration of U2–U6 helix Ib, U4–U6 stem I or both[19] (**Fig. 3c**). Remarkably, a mutation at the predicted base-triple partner, U6 A53C, suppressed not only the sick phenotype of A59C and the lethality of A59G but also the lethality of A59U—all without U2–U6 helix Ib repair (**Fig. 3c** and **Supplementary Fig. 1c**). To our knowledge, this marks the first observed suppression of A59U (**Supplementary Note 4**). Although A53C suppressed all three alleles at position A59, suppression was position specific (**Fig. 3d** and **Supplementary Fig. 1d**). Additionally, only the A53C allele suppressed all three A59 point mutations (**Fig. 3c**), thus suggesting a specific mechanism of suppression (described below). Together, these data, especially regarding the positional specificity, provide evidence for a base-triple interaction between A53 of the ACAGAGA sequence and A59 of the AGC triad.

If the suppression of AGC-triad mutations is direct, via formation of compensatory base-triple interactions, as the allele specificity and position specificity of our data strongly imply, then suppressor combinations should be capable of forming similar base-triple interactions. Consequently, we assessed the structural similarity between potential suppressor base triples and wild-type base triples, modeled on the basis of the group II structure[7,11]. Where appropriate, to guide this comparison, we used published matrices enumerating the many possible base-base interactions observed crystallographically or predicted by modelling[29]. Two of the three group II–intron triples are unusual[11], and the third triple, although resembling analogous triples, is not strictly isosteric with any of these interactions[29]. Two base-base interactions are generally considered to be similar if the configurations conserve the distance between their linkages to the sugar-phosphate backbone. We focused specifically on the C1′-C1′ distance between the AGC-triad residues and their predicted base-triple partners (**Figs. 2c** and **3e**,**f**) because this distance probably influences catalytic-metal positioning by the AGC triad[4].

For each of the predicted base triples, we discovered a suppressor base triple that could form interactions that resembled the configuration of the wild-type base triple, predicted from the group II structure (**Figs. 2c** and **3e**,**f** and **Supplementary Note 5**). For example, with suppression of the U2-U6 G21C C61G double mutant by U6 U80C (**Fig. 2a**), O6 of C61G could interact with N4 of U80C to form a similar base triple (**Fig. 2c**). Similarly, for the base triple involving G52 and G60, the C1′-C1′ distance for our proposed suppressor base triple is remarkably similar to that of the predicted wild-type base triple (within 0.4 Å, **Supplementary Table 2**). For the final base triple, we can in some cases model a plausible suppressor base triple (for example, **Fig. 3f**), but the capacity of the A53C mutation to suppress generally suggests that it might do so by forming a base-neutral interaction with the phosphate backbone of A59, just as the equivalent residue of the group II intron interacts with the backbone[11] (**Fig. 1c** and **Supplementary Notes 5** and **6**). This analysis suggests that the base-triple suppressor combinations probably act directly by restoring a configuration of the bases similar to that observed in the wild-type context.

Overall, our analysis is consistent with a mechanism of suppression in which the new suppressor combinations permit growth by forming base-triple interactions structurally similar to those predicted for the wild-type context. Further, as has been observed previously for other triple-helix interactions[27], we observed that a mutation that suppressed disruption of one base triple exacerbated disruption of another base triple (in 75% of the tests, **Supplementary Table 1**)—a result that is consistent with triplex formation, because these tests would disrupt two, rather than one, of the three triples. Thus, although our data are not sufficient to define base-triple interactions at atomic

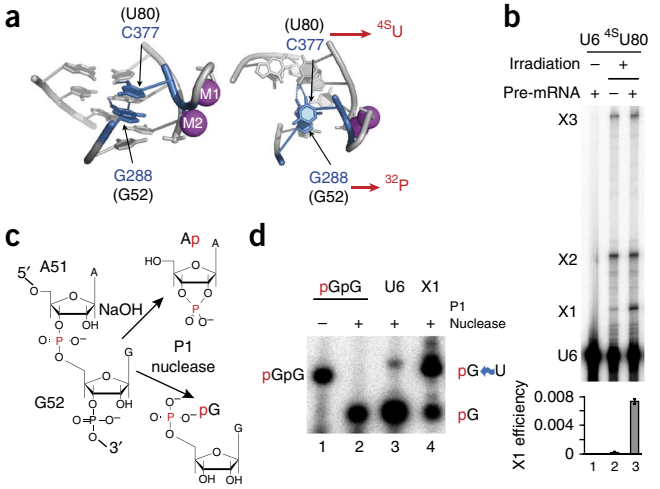

Figure 4 The U6 triplex forms *in vitro*. (**a**) Stacking interaction between C377 and G288, as observed in the group II intron crystal structure (PDB 4FAQ[8]). Left, side view; right, top view. Equivalent spliceosome residues are indicated in parentheses. The positions of the 4-thiouridine (^{4S}U) and of the radioactive label (^{32}P) are indicated in red. (**b**) Denaturing PAGE analysis of U6 ^{4S}U80 recovered from *in vitro* splicing reactions after UV irradiation. Where indicated, unlabeled *ACT1* pre-mRNA was present in the reactions. The U6 cross-links (X1, X2 and X3) are indicated. The efficiency of X1 formation is quantified below the gel; error bars, s.d. from three technical replicates. (**c**) Predicted products for P1 nuclease (which is able to cleave 5′ of UV-cross-linked RNA residues[46]) and NaOH digestion. (**d**) Denaturing PAGE analysis of RNA products after P1 nuclease digestion of un–cross-linked U6 or X1 excised from a gel like that shown in **b**. A 5′-[^{32}P]-pGpG dinucleotide was also digested with P1 as a size marker. Curvy blue arrow signifies a cross-link; ^{32}P is indicated in red. Full gels are in **Supplementary Figure 8a**,**b**.

resolution, which is currently not feasible for the spliceosome, our data establish evidence that the residual function of the AGC triad, not accounted for by pairing with U2, U4 or U6, is to form a triplex interaction, in the context of helix Ib, with the bulge of the U6 ISL and the ACAGAGA region of U6, the latter of which binds the 5′ splice site.

Physical evidence for the U6 triplex

As a result of triple-helix formation in domain V, two of the base-triple partners (C377 and G288) stack through their base rings (**Fig. 4a**). To investigate whether the corresponding positions in U6 (U80 and G52) form a similar stacking interaction, we designed a cross-linking assay. We reconstituted U6-depleted extract with a synthetic U6 (U6 ^{4S}U80) containing 4-thiouridine at U80 and a single radioactive label at G52 (**Fig. 4a** and **Supplementary Fig. 2a**). If these two bases stack, UV irradiation should induce formation of a covalent linkage between U80 and G52 (ref. 30), with the site-specific radiolabel facilitating identification of such a linkage.

We detected three major cross-links that were dependent on both UV irradiation and 4-thiouridine (**Fig. 4b** and **Supplementary Fig. 2b**), including an extract-independent cross-link (X2) and the previously reported U4-U6 cross-link involving U80 (X3; ref. 31 and **Fig. 4b**; characterization of X2 and X3 in **Supplementary Fig. 2c–e**). Most importantly, we observed extract-dependent and pre-mRNA–stimulated formation of a cross-link migrating closely to un–cross-linked U6 (X1, **Fig. 4b** and **Supplementary Fig. 2c**). To determine whether this reflected intramolecular cross-linking, we performed P1 nuclease digestion, which degrades RNA to single nucleotides with 5′-monophosphates[32] (**Fig. 4c**). Whereas un–cross-linked U6 digested to radiolabeled mononucleotide, reflecting formation of 5′-pG (p, phosphate; **Fig. 4c**,**d**), X1 digested to a species migrating more slowly than the mononucleotide and close to a dinucleotide standard (**Fig. 4d**), thus providing evidence that G52 cross-linked to U80. In contrast, when we performed RNA hydrolysis, which yields single nucleotides with cyclic 3′-monophosphates (**Fig. 4c**), both un–cross-linked U6 and X1 yielded radiolabeled mononucleotide, thus reflecting formation of Ap-3′ (**Supplementary Note 7** and **Supplementary Fig. 2f**,**g**) and thereby ruling out that U80 cross-linked to A51. We conclude that X1 results from cross-linking between G52 and U80. Given an analogous cross-link between equivalent positions in the group II intron, which stack in the domain V triplex[13], and the chemical mechanism of 4-thiouridine cross-linking (**Supplementary Note 8**), the simplest explanation for our observed cross-link is that U80 and G52 stack in the context of a triplex structure. Thus, this provides physical evidence for a group II intron–like U6 triplex in the spliceosome.

The NTC promotes U6-triplex formation

The cross-linking of U80 to G52 allowed us to investigate when the U6 triplex forms during the splicing cycle. To do so, we induced cross-linking of U6 ^{4S}U80 spliceosomes after stalling at defined stages through the use of dominant-negative mutations of DEAH-box ATPases known to promote conformational rearrangements during

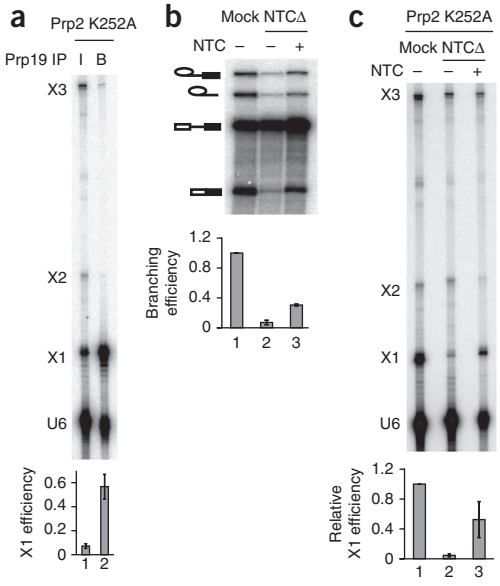

Figure 5 The NTC promotes formation of the U6 triplex. (**a**) Denaturing PAGE analysis of radiolabeled U6 ^{4S}U80 extracted from a splicing reaction after UV irradiation and immunoprecipitation via Prp19p. 5% of the input (I) and all of the beads (B) were analyzed. (**b**) Denaturing PAGE analysis of radiolabeled *ACT1* pre-mRNA after *in vitro* splicing in extracts depleted of the NTC (NTCΔ) with or without addition of purified yeast NTC[36]. (**c**) Denaturing PAGE analysis of U6 ^{4S}U80 recovered from *in vitro* splicing reactions after UV irradiation. Splicing of unlabeled *ACT1* pre-mRNA was performed in extracts depleted of the NTC (NTCΔ) and reconstituted with radiolabeled U6 ^{4S}U80. In **a** and **c**, rPrp2p-K252A was added to stall spliceosomes immediately after NTC binding and before Prp2p-dependent activation. In **a** and **c**, the efficiency of X1 formation is quantified below the gel; in **c**, the X1 efficiency was normalized to the mock-depleted reactions for individual experiments; in **b**, the splicing efficiency, normalized to the mock-depleted reaction, is quantified below the gel. Error bars, s.d. from three technical replicates. Full gels are in **Supplementary Figure 8c–e**.

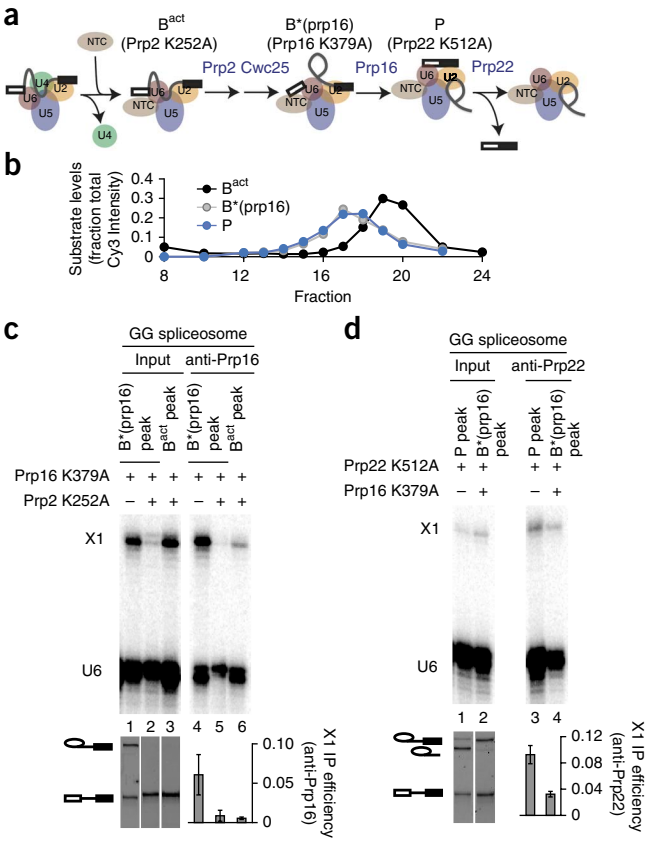

Figure 6 The U6 triplex is present at the branching and exon-ligation stages of splicing. (**a**) General splicing pathway highlighting the complexes used to probe for the triplex at the catalytic stages. Individual small nuclear ribonucleoproteins are shown as ovals. The relevant complexes are labeled; the dominant-negative ATPase mutant that was added to induce accumulation of specific complexes is indicated in parentheses. (**b**) Glycerol-gradient sedimentation profile of the complexes used for cross-linking. Spliceosomes containing U6 ^{4S}U80 were assembled on Cy3-labeled *UBC4* pre-mRNA and then sedimented. For each gradient fraction, the Cy3-labeled pre-mRNA, lariat intermediate or excised intron, corresponding to B^{act}, B*(prp16) or P complex, respectively, is quantified as a fraction of the total Cy3 signal. (**c**,**d**) Denaturing PAGE analysis of radiolabeled U6 ^{4S}U80 recovered after complex isolation, UV irradiation, and immunoprecipitation via Prp16p (**c**) or Prp22p (**d**). The indicated spliceosomal complexes were UV irradiated and immunoprecipitated after isolation from peak glycerol-gradient fractions, as illustrated in **b**. GG spliceosome, glycerol gradient–isolated spliceosome; input, before immunoprecipitation; anti-Prp16 and anti-Prp22, after immunoprecipitation. The bottom panels in **c** and **d** show the *UBC4* pre-mRNA substrate present in the fractions used for immunoprecipitation, detected by Cy3. The X1 immunoprecipitation efficiency (relative to X1 present in the input) is quantified in each panel. Error bars, s.d. from three technical replicates. Full gels are in **Supplementary Figure 8f–h**.

in vitro splicing[1]. Unexpectedly, we detected X1 at very high levels in B^{act} spliceosomes, which are stalled by a dominant-negative Prp2p mutant (rPrp2p-K252A) at the final ATP-dependent step in spliceosome activation (**Fig. 5a** and **Supplementary Fig. 3**), thus providing evidence that the U6 triplex forms before the final stage in catalytic activation. Strikingly, immunoprecipitation via Prp19p revealed that more than 50% of U6 in B^{act} spliceosomes formed the X1 cross-link in extract (**Fig. 5a**). Such high cross-linking efficiency requires stacking of the residues involved[33–35] and suggests that the U6 triplex is a defining feature of spliceosomes poised for final activation.

Given triplex formation in B^{act} spliceosomes, we asked whether triplex formation required the Prp19p-associated complex (NTC), which is necessary for stabilization of B^{act} spliceosomes after release of U4 snRNA[36]. Depletion of the NTC from splicing extracts resulted in a strong reduction in X1, and purified NTC rescued the cross-link (**Fig. 5b**,**c**), thus defining a role for the NTC in stabilizing the U6 base-triple interactions (additional information in **Supplementary Fig. 4** and **Supplementary Note 9**). Further, given the involvement of the ACAGAGA sequence in the U6 triplex, our data indicate that the 5′ splice site docks into the catalytic core at the stage of NTC binding (described in Discussion).

The U6 triplex is present at branching and exon ligation

Biochemical data and crystal structures of the group II intron imply a role for the domain V triplex in both catalytic steps[7,8,13,20]. Further, we have shown in the spliceosome that catalytic-metal ligands that would be organized by the triplex function in both catalytic steps[4]. Consequently, we tested whether the U6 triplex is present during each catalytic step.

To test for the triplex at the branching stage, we stalled spliceosomes just after branching by addition of a dominant-negative Prp16p mutant that remains bound to the spliceosome (rPrp16p-K379A) and isolated from glycerol gradients the resulting spliceosome complexes, which had catalyzed branching but had not undergone the Prp16p-dependent rearrangement (denoted B*(prp16)) (**Fig. 6a**,**b**). UV irradiation of these spliceosomes induced high levels of X1 (**Fig. 6c**), thus suggesting the presence of the triplex at the branching stage. To test this interpretation further, we used Prp16p as a specific immunoaffinity handle for X1 in genuine B*(prp16) spliceosomes, because Prp16p binds stably to this complex in a Prp2p-dependent manner just before branching[37] and dissociates just after branching[38]. X1 immunoprecipitated efficiently from the B*(prp16) peak (**Fig. 6c** and **Supplementary Fig. 5**). By contrast, when we stalled spliceosomes before branching at the Prp2p stage, X1 did not efficiently immunoprecipitate from the B^{act} peak, thus indicating that the immunoprecipitation of X1 via Prp16p was specific for the B*(prp16) complex (**Fig. 6c** and **Supplementary Note 10**).

To test for the triplex at the exon-ligation stage, we stalled spliceosomes just after exon ligation by addition of rPrp22p-K512A and isolated from glycerol gradients the resulting complexes (denoted P) that had not released the mRNA (**Fig. 6a**,**b**). UV irradiation of these complexes induced the X1 cross-link (**Fig. 6d**), thus suggesting the presence of the triplex at the exon-ligation stage. To test this implication further, we used Prp22p as a specific immunoaffinity handle for P-complex spliceosomes, because Prp22p binds stably to only this complex, in a manner dependent on Prp16p, Slu7p and Prp18p just before exon ligation[37,39], and dissociates just after exon ligation[40]. When spliceosomes were stalled after exon ligation, we observed substantial immunoprecipitation of X1 from fractions of the P peak (**Fig. 6d**). By contrast, when spliceosomes were stalled just after branching, X1 immunoprecipitated three-fold less efficiently from equivalent fractions (**Fig. 6d**), even though the accumulating B*(prp16) complexes and associated X1 cross-link migrated in the same fractions (**Fig. 6b**); thus, the immunoprecipitation of X1 via Prp22p was specific for the P complex. We conclude that U80 and G52 also stack at the exon-ligation stage. These results indicate that the U6 catalytic triplex is present during both catalytic steps of splicing and provides a structural framework for the organization of the U6 ligands for the catalytic metals that function during both reactions[4].

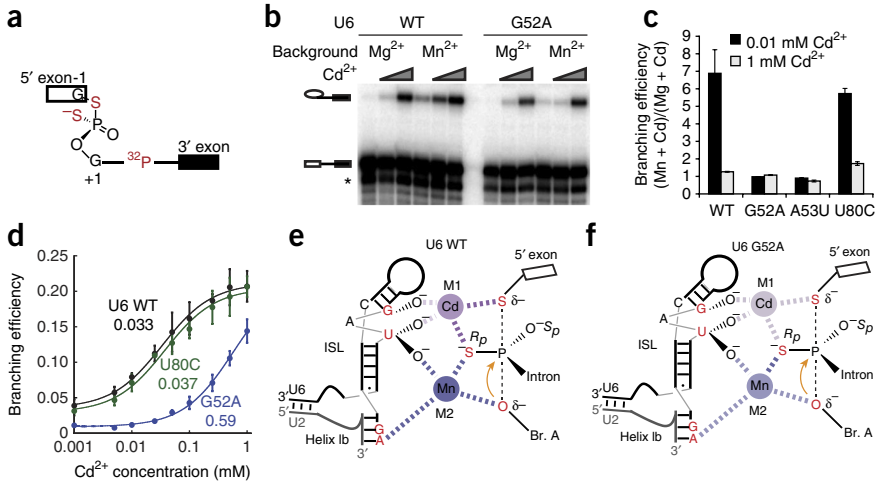

Figure 7 The U6 triplex promotes catalytic-metal binding during branching. (**a**) Diagram of the 3′S-PS(R_P) pre-mRNA. (**b**) Denaturing PAGE analysis of splicing of the 3′S-PS(R_P) pre-mRNA catalyzed by affinity-purified spliceosomes in the presence of the indicated combinations of metals. In **b**, the band marked with an asterisk results from exonucleolytic degradation that stops at the sulfur. (**c**) Quantification of Mn^{2+} potentiation of Cd^{2+}-dependent rescue of branching of the 3′S-PS(R_P) pre-mRNA by spliceosomes containing the indicated U6 variants. Mn^{2+} potentiation is quantitated relative to Mg^{2+}. Bars indicate ranges of two technical replicates. (**d**) Titration curves showing efficiency of Cd^{2+}-mediated rescue of branching of the 3′S-PS(R_P) pre-mRNA by affinity-purified spliceosomes reconstituted with the indicated U6 variants. Hill fits to the data, assuming one rescuing metal, are shown (solid lines). The apparent transition midpoints are indicated below the label of each U6 variant. Error bars, s.d. of three independent replicates. (**e**,**f**) Diagrams showing predicted catalytic-metal binding by spliceosomes containing U6 WT (**e**) or U6 G52A (**f**). Relevant U6 ligands and the nucleophile are colored red. Metals are colored magenta (Cd^{2+}) and blue (Mn^{2+}), and their interactions with specific U6 ligands are depicted as dashed lines, with differential shading intensity illustrating differences in the expected strength of interaction with oxygen versus sulfur, as inferred from studies with model compounds[47]. Shading of metals bound at M1 and M2 is further adjusted to reflect experimental observations. Br. A, branch-site A nucleophile.

The U6 triplex promotes catalytic-metal binding

The U6 triplex provides a structural mechanism for positioning the two catalytic metals[4] in a proper configuration for phosphoryl transfer (**Fig. 1**). To determine whether the U6 triplex promotes catalytic-metal binding, we tested whether mutations predicted to disrupt the triplex impair catalytic-metal binding. The mutations G52A and A53U in U6 confer lethality or a growth defect *in vivo* (**Fig. 3**) and cause exon-ligation defects *in vitro* (**Supplementary Fig. 6** and **Supplementary Note 11**); we infer that these phenotypes result from disruption of their base-triple interactions with the AGC triad. We assayed the impact of these mutations on catalytic-metal binding during branching by using a pre-mRNA substrate that bears sulfur substitutions at both the leaving group and the nonbridging *pro*-R_P phosphoryl oxygen at the 5′ splice site (3′S-PS(R_P)), which disrupt interactions with both catalytic Mg^{2+} ions[4] (**Fig. 7a**). In a background of Mg^{2+}, these interactions can be rescued by binding of two thiophilic Cd^{2+} ions at high concentrations[4]. In a background of Mn^{2+}, which is more thiophilic than Mg^{2+}, Cd^{2+} can rescue at lower concentrations, because Mn^{2+} can populate one site (M2) and enable high-affinity binding of Cd^{2+} to the other site, M1 (ref. 4; **Fig. 7e**). Thus, at limiting Cd^{2+} concentrations (for example, 10 μM), Mn^{2+} potentiates the efficiency of branching for the 3′S-PS(R_P) substrate (compared to the efficiency observed in Mg^{2+}; **Fig. 7b**,**c**). Remarkably, in a background of Mn^{2+}, mutations in U6 predicted to destabilize the base-triple interactions (G52A and A53U) compromised Cd^{2+}-dependent rescue of the 3′S-PS(R_P) substrate (**Fig. 7b**,**c**). Indeed, compared to U6 wild type, U6 G52A increased the apparent transition midpoint for Cd^{2+} rescue of the 3′S-PS(R_P) substrate by more than ten-fold (**Fig. 7d**). These data indicate that destabilization of the U6 G52•U6 G60–U2 C22 base triple disrupted metal binding at the catalytic core (**Fig. 7f**). In agreement with this interpretation, the strong G52A-induced defect in branching at low Cd^{2+} concentrations, relative to branching in wild type, was almost completely suppressed at high Cd^{2+} concentrations (**Fig. 7d**). In contrast, U6 U80C, predicted to maintain the proper configuration of the U6 triplex[11], did not compromise Cd^{2+} rescue of the 3′S-PS(R_P) substrate at limiting Cd^{2+} (**Fig. 7c**) and did not affect the transition

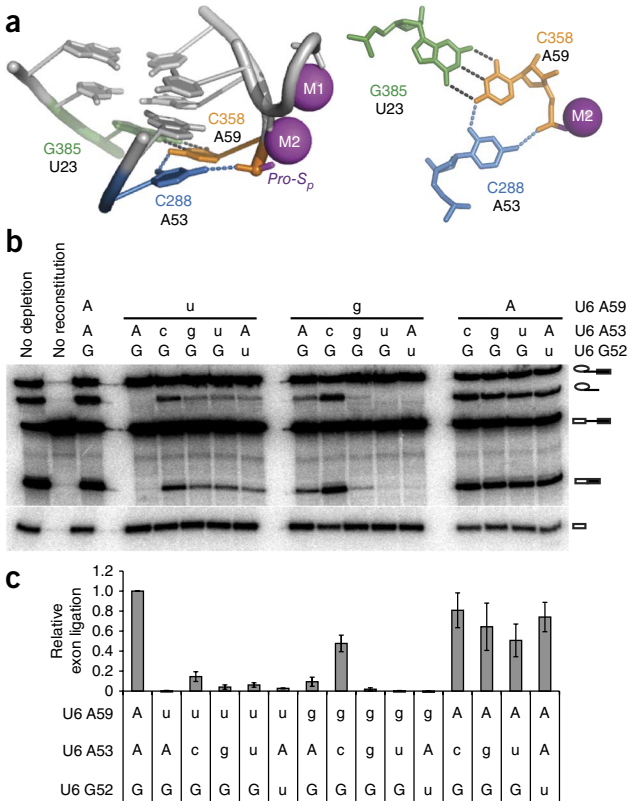

Figure 8 The U6 triplex promotes exon ligation *in vitro*. (**a**) Configuration of the C288•C358-G385 base triple in the group II intron (PDB 4FAQ[8]), equivalent to the spliceosomal U6 A53•U6 A59–U2 U23 base triple. Left, side view; right, top view. (**b**) Denaturing PAGE analysis of splicing of *ACT1* pre-mRNA in extracts reconstituted with the indicated U6 variants. Uppercase indicates wild-type allele. Lowercase indicates mutant allele. (**c**) Quantification of exon ligation for the indicated U6 variants, normalized to wild-type U6; exon ligation was calculated as mRNA/lariat intermediate[19]. Error bars, s.d. of two independent experiments and two technical replicates for each experiment. The efficiency of branching was within 15% of wild type for all U6 variants (quantification not shown). Full gel is in **Supplementary Figure 8i**.

midpoint for rescue by Cd^{2+} (**Fig. 7d**). Together, these results establish that the triplex promotes binding of catalytic metals and define an essential role for the U6 triplex during catalysis of branching.

The U6 triplex promotes exon ligation

Because our cross-linking experiments implied that the triplex is present during exon ligation (**Fig. 6d**), we tested whether exon ligation required the triplex. Of the bases involved in the triplex, only A59 shows a specific defect in exon ligation when mutated[18]. Our *in vivo* results suggest that A59 forms a base-triple interaction with A53, similar to that observed for the equivalent positions in the group II intron (**Figs. 3c** and **8a**). Therefore, we asked whether the exon-ligation defects conferred by U6 A59 mutations could be suppressed by mutations at U6 A53. Strikingly, the A53C mutation strongly improved exon-ligation efficiency for both A59U and A59G (**Fig. 8b**,**c**). Suppression was allele specific, because A59G was enhanced by rather than suppressed by other A53 mutations, and A59U was only mildly suppressed by other A53 mutations. Importantly, the observed suppression was also position specific, because neither A59G nor A59U was substantially suppressed by a mutation at the neighboring G52 (**Fig. 8b**,**c**), which nevertheless suppressed the exon-ligation defect conferred by a mutation at its base-triple partner G60 (**Supplementary Fig. 7a**,**b**). A53C also suppressed the exon-ligation defect of compromised pre-mRNA reporters both *in vitro* and *in vivo* (**Supplementary Fig. 7d**,**e**). Overall the allele- and position-specific suppression of exon-ligation defects that we observed *in vitro* explicitly paralleled the suppression that we observed *in vivo* (**Fig. 3a**,**c**). We infer that the *in vitro* suppression, as that *in vivo*, reflects the formation of a group II–like base triple that includes an interaction between A53C and the backbone of A59 (**Fig. 8a**). Together, these results indicate that the U6 triplex not only forms at the exon-ligation stage (**Fig. 6d**) but also functions at this catalytic stage both *in vivo* and *in vitro*.

DISCUSSION

Here we provide evidence for the formation of a catalytic triplex in the spliceosome, analogous to the metal-binding catalytic triplex of group II introns (**Fig. 1**). Specifically, despite the dynamic nature of the AGC triad[15], the role for the triad in catalysis[4] and the unusual and discontinuous nature of the group II intron triplex[7,8], U6 mutations within the ACAGAGA and ISL bulged elements suppressed growth defects of AGC-triad mutants in the context of U2–U6 helix Ib in an allele- and position-specific manner at all three triples, thus providing independent and corroborative evidence for tertiary interactions between these highly conserved U6 residues (**Figs. 2** and **3**). By site-directed cross-linking, we revealed physical evidence for the U6 triplex (**Fig. 4**) and showed that, strikingly, the triplex forms upon NTC binding (**Fig. 5**), before the last ATP-dependent activation step, thus suggesting that the catalytic core is already formed at the precatalytic stage. Finally, we established that the catalytic triplex is present at both catalytic stages of splicing (**Fig. 6**), promotes both branching and exon ligation and has an essential role in positioning catalytic metals (**Figs. 7** and **8**). These data establish clear evidence that a catalytic triplex forms at the heart of the active spliceosome. The triple helix provides a mechanism by which the spliceosome structures U6 snRNA in a conformation competent to bind the two divalent metals that catalyze splicing[4]. Furthermore, the triplex provides a rationale for how the spliceosome recruits the pre-mRNA reactive phosphates to this metal-binding core for catalysis (described below). Finally, our results extend the deep mechanistic parallels between the spliceosome and group II introns and further support the likelihood of a common evolutionary precursor[5].

The AGC triad was identified early on as a strictly conserved element highly sensitive to mutation[15] and was later shown to base-pair with U4 (ref. 25) in assembling spliceosomes and with U2 in activated spliceosomes[15,17,19]. With this work, we show that in activated spliceosomes the triad interacts not only with U2 but also with distal regions in U6 to yield base triples (**Figs. 2–4**). Indeed, the triplex, with the AGC triad at the backbone, may explain the asymmetric phenotypes in U2–U6 helix Ib—the strong phenotypes in U6 and the weak phenotypes in U2 (refs. 15,19)—an asymmetry that is mirrored in the U6-U6 triple interactions.

Because the two metal ions required for splicing catalysis are bound by the AGC triad and the bulge of the U6 ISL[4], the catalytic triplex provides a mechanism to juxtapose these two metal ion–binding sites in U6 for two-metal-ion catalysis. Indeed, our results indicate that the integrity of the U6 triplex is essential for proper metal positioning by the catalytic core, as observed during branching (**Fig. 7**).

The catalytic triplex also provides a mechanism for recruiting the 5′ splice site to the metal-binding core. The 5′ splice site is defined through base-pairing interactions with the 5′ end of the ACAGAGA sequence of U6 (refs. 21,22). Because the 3′ end of the ACAGAGA sequence participates directly in the triplex (**Fig. 1a**), the triplex probably recruits the U6–5′-splice-site interaction to the catalytic core for branching. The timing of triplex formation supports this hypothesis. By site-directed cross-linking, we found that the triplex forms before the final catalytic activation step of the spliceosome, mediated by Prp2p; the triplex forms after the release of U4 snRNA from U6 and upon binding of the NTC and associated factors to the spliceosome (**Fig. 5**). Because the NTC consolidates interactions of the exonic region of the 5′ splice site with U5 and promotes correct pairing between the intronic region of the 5′ splice site and the ACAGAGA sequence of U6 (ref. 41), our results suggest coupling between binding of the 5′ splice site and formation of a catalytic configuration of the RNA core. Similarly, during the exon-ligation stage the integrity of the triplex may be coupled to recruitment of the 3′ splice site (**Supplementary Note 12**). Such coupling highlights the dependence of the catalytic core on substrate binding and may allow sampling and proofreading of the substrate through inspection of the catalytic core at subsequent steps in the splicing pathway. Indeed, downstream of NTC binding, both Prp2p and Prp16p have been implicated in proofreading, in part through destabilization of a weakly formed catalytic core[17,42,43].

Before branching, Prp2p has been implicated in destabilizing the catalytic core, including the triplex, to promote on-pathway rearrangements[43]. Our *in vitro* analysis indicates that the U6 triplex must restabilize to promote branching (**Figs. 6c** and **8** and **Supplementary Fig. 7**). Cwc2p stabilizes the triplex before Prp2p activity (**Supplementary Fig. 4**), and after Prp2p action, when Cwc2p becomes essential for branching, Cwc2p interacts with the U6 ISL[2]. Thus, Cwc2p may act to restabilize the catalytic core for branching catalysis.

After branching, Prp16p has been implicated in destabilizing the catalytic core[17], probably to accommodate substrate repositioning—the replacement of the branch site with the 3′ splice site at the catalytic metal–binding site[4]. We found that, consistently with a role in destabilizing the helix Ib component of the catalytic core[17], mutations predicted to destabilize the U6 triplex (U6 A53C and U6 A53G) suppressed a hypomorphic allele of *prp16* (**Supplementary Fig. 7c**). These data imply that Prp16p destabilizes the U6 triplex after the spliceosome has catalyzed branching. Interestingly, the transition from branching to exon ligation requires disruption of the U6–5′-splice-site pairing[44]. Thus, our data also suggest that disruption of the U6–5′-splice-site pairing after branching is coupled to destabilization of the U6 triplex.

As we have found for other elements of the catalytic core[17,45], here we found evidence that the triplex is destabilized only transiently during the catalytic stage; the triplex reforms at the exon-ligation stage (**Fig. 6d** and **Supplementary Fig. 7**) and is necessary for efficient exon ligation (**Fig. 8**). Interestingly, although the catalytic triplex of the group II intron similarly appears to function in both catalytic conformations, the group II triplex has also been suggested to disrupt transiently between the two steps of splicing, to allow substrate repositioning[8].

Overall our results indicate that the spliceosomal catalytic core shares remarkable structural and functional similarity, if not also evolutionary origins[5], with the catalytic core of group II self-splicing introns. Thus, these data underscore evidence that splicing catalysis is performed by an RNA-based catalytic core[4] stabilized by a complex protein scaffold[2,3].

METHODS

Methods and any associated references are available in the online version of the paper.

Note: Any Supplementary Information and Source Data files are available in the online version of the paper.

ACKNOWLEDGMENTS

We thank S.-C. Cheng (Academia Sinica) for strains; C. Guthrie (University of California, San Francisco) and B. Schwer (Weill Cornell Medical College) for antibodies; D. Semlow (Staley laboratory) for recombinant proteins and Cy3-labeled *UBC4* pre-mRNA; and members of the Staley and Piccirilli laboratories for critical discussions and comments on the manuscript. M.A.M. was supported by US National Institutes of Health training grant (T32 GM007183); this work was funded by a grant from the US National Institutes of Health (R01GM088656) to J.P.S. and J.A.P.

AUTHOR CONTRIBUTIONS

S.M.F., M.A.M., J.A.P. and J.P.S. designed the study; M.A.M. performed the *in vivo* genetics; S.M.F. performed the *in vitro* cross-linking and biochemistry experiments as well as experiments in **Supplementary Figure 7**, which were initiated by M.A.M.; and S.M.F. and J.P.S. wrote the paper with input from M.A.M. and J.A.P.

COMPETING FINANCIAL INTERESTS

The authors declare no competing financial interests.

1. Wahl, M.C., Will, C.L. & Lührmann, R. The spliceosome: design principles of a dynamic RNP machine. *Cell* **136**, 701–718 (2009).
2. Rasche, N. *et al.* Cwc2 and its human homologue RBM22 promote an active conformation of the spliceosome catalytic centre. *EMBO J.* **31**, 1591–1604 (2012).
3. Galej, W.P., Oubridge, C., Newman, A.J. & Nagai, K. Crystal structure of Prp8 reveals active site cavity of the spliceosome. *Nature* **493**, 638–643 (2013).
4. Fica, S.M. *et al.* RNA catalyses nuclear pre-mRNA splicing. *Nature* **503**, 229–234 (2013).
5. Cech, T.R. The generality of self-splicing RNA: relationship to nuclear mRNA splicing. *Cell* **44**, 207–210 (1986).
6. Steitz, T.A. & Steitz, J.A. A general two-metal-ion mechanism for catalytic RNA. *Proc. Natl. Acad. Sci. USA* **90**, 6498–6502 (1993).
7. Toor, N., Keating, K.S., Taylor, S.D. & Pyle, A.M. Crystal structure of a self-spliced group II intron. *Science* **320**, 77–82 (2008).
8. Marcia, M. & Pyle, A.M. Visualizing group II intron catalysis through the stages of splicing. *Cell* **151**, 497–507 (2012).
9. Sontheimer, E.J., Gordon, P.M. & Piccirilli, J.A. Metal ion catalysis during group II intron self-splicing: parallels with the spliceosome. *Genes Dev.* **13**, 1729–1741 (1999).
10. Gordon, P.M., Fong, R. & Piccirilli, J.A. A second divalent metal ion in the group II intron reaction center. *Chem. Biol.* **14**, 607–612 (2007).
11. Keating, K.S., Toor, N., Perlman, P.S. & Pyle, A.M. A structural analysis of the group II intron active site and implications for the spliceosome. *RNA* **16**, 1–9 (2010).
12. Mikheeva, S., Murray, H.L., Zhou, H., Turczyk, B.M. & Jarrell, K.A. Deletion of a conserved dinucleotide inhibits the second step of group II intron splicing. *RNA* **6**, 1509–1515 (2000).
13. de Lencastre, A. & Pyle, A.M. Three essential and conserved regions of the group II intron are proximal to the 5′-splice site. *RNA* **14**, 11–24 (2008).
14. Jacquier, A. & Michel, F. Base-pairing interactions involving the 5′ and 3′-terminal nucleotides of group II self-splicing introns. *J. Mol. Biol.* **213**, 437–447 (1990).
15. Madhani, H.D. & Guthrie, C. A novel base-pairing interaction between U2 and U6 snRNAs suggests a mechanism for the catalytic activation of the spliceosome. *Cell* **71**, 803–817 (1992).
16. Sun, J.S. & Manley, J.L. A novel U2–U6 snRNA structure is necessary for mammalian mRNA splicing. *Genes Dev.* **9**, 843–854 (1995).
17. Mefford, M.A. & Staley, J.P. Evidence that U2/U6 helix I promotes both catalytic steps of pre-mRNA splicing and rearranges in between these steps. *RNA* **15**, 1386–1397 (2009).
18. Fabrizio, P. & Abelson, J.J. Two domains of yeast U6 small nuclear RNA required for both steps of nuclear precursor messenger RNA splicing. *Science* **250**, 404–409 (1990).
19. Hilliker, A.K. & Staley, J.P. Multiple functions for the invariant AGC triad of U6 snRNA. *RNA* **10**, 921–928 (2004).
20. Chanfreau, G. & Jacquier, A. Catalytic site components common to both splicing steps of a group II intron. *Science* **266**, 1383–1387 (1994).
21. Lesser, C.F. & Guthrie, C. Mutations in U6 snRNA that alter splice site specificity: implications for the active site. *Science* **262**, 1982–1988 (1993).
22. Kandels-Lewis, S. & Séraphin, B. Role of U6 snRNA in 5′ splice site selection. *Science* **262**, 2035–2039 (1993).
23. Anokhina, M. *et al.* RNA structure analysis of human spliceosomes reveals a compact 3D arrangement of snRNAs at the catalytic core. *EMBO J.* **32**, 2804–2818 (2013).
24. Sashital, D.G., Cornilescu, G., McManus, C.J., Brow, D.A. & Butcher, S.E. U2–U6 RNA folding reveals a group II intron-like domain and a four-helix junction. *Nat. Struct. Mol. Biol.* **11**, 1237–1242 (2004).
25. Brow, D.A. & Guthrie, C. Spliceosomal RNA U6 is remarkably conserved from yeast to mammals. *Nature* **334**, 213–218 (1988).
26. Qiao, F. & Cech, T.R. Triple-helix structure in telomerase RNA contributes to catalysis. *Nat. Struct. Mol. Biol.* **15**, 634–640 (2008).
27. Mitton-Fry, R.M., DeGregorio, S.J., Wang, J., Steitz, T.A. & Steitz, J.A. Poly(A) tail recognition by a viral RNA element through assembly of a triple helix. *Science* **330**, 1244–1247 (2010).
28. Cash, D.D. *et al.* Pyrimidine motif triple helix in the *Kluyveromyces lactis* telomerase RNA pseudoknot is essential for function *in vivo*. *Proc. Natl. Acad. Sci. USA* **110**, 10970–10975 (2013).
29. Leontis, N.B., Stombaugh, J. & Westhof, E. The non-Watson-Crick base pairs and their associated isostericity matrices. *Nucleic Acids Res.* **30**, 3497–3531 (2002).
30. Sontheimer, E.J. Site-specific RNA crosslinking with 4-thiouridine. *Mol. Biol. Rep.* **20**, 35–44 (1994).
31. Ryan, D.E. *et al.* New tertiary constraints between the RNA components of active yeast spliceosomes: a photo-crosslinking study. *RNA* **10**, 1251–1265 (2004).
32. Volbeda, A., Lahm, A., Sakiyama, F. & Suck, D. Crystal structure of *Penicillium citrinum* P1 nuclease at 2.8 A resolution. *EMBO J.* **10**, 1607–1618 (1991).
33. Yaniv, M., Favre, A. & Barrell, B.G. Structure of transfer RNA: evidence for interaction between two non-adjacent nucleotide residues in tRNAVal1 from *Escherichia coli*. *Nature* **223**, 1331–1333 (1969).
34. Grishaev, A., Ying, J., Canny, M.D., Pardi, A. & Bax, A. Solution structure of $tRNA^{Val}$ from refinement of homology model against residual dipolar coupling and SAXS data. *J. Biomol. NMR* **42**, 99–109 (2008).
35. Favre, A., Saintomé, C., Fourrey, J.L., Clivio, P. & Laugâa, P. Thionucleobases as intrinsic photoaffinity probes of nucleic acid structure and nucleic acid-protein interactions. *J. Photochem. Photobiol. B* **42**, 109–124 (1998).
36. Chan, S.-P., Kao, D.-I., Tsai, W.-Y. & Cheng, S.-C. The Prp19p-associated complex in spliceosome activation. *Science* **302**, 279–282 (2003).
37. Ohrt, T. *et al.* Molecular dissection of step 2 catalysis of yeast pre-mRNA splicing investigated in a purified system. *RNA* **19**, 902–915 (2013).
38. Schwer, B. & Guthrie, C. PRP16 is an RNA-dependent ATPase that interacts transiently with the spliceosome. *Nature* **349**, 494–499 (1991).
39. James, S.-A., Turner, W. & Schwer, B. How Slu7 and Prp18 cooperate in the second step of yeast pre-mRNA splicing. *RNA* **8**, 1068–1077 (2002).
40. Schwer, B. & Gross, C.H. Prp22, a DExH-box RNA helicase, plays two distinct roles in yeast pre-mRNA splicing. *EMBO J.* **17**, 2086–2094 (1998).
41. Chan, S.-P. & Cheng, S.-C. The Prp19-associated complex is required for specifying interactions of U5 and U6 with pre-mRNA during spliceosome activation. *J. Biol. Chem.* **280**, 31190–31199 (2005).
42. Semlow, D.R. & Staley, J.P. Staying on message: ensuring fidelity in pre-mRNA splicing. *Trends Biochem. Sci.* **37**, 263–273 (2012).
43. Wlodaver, A.M. & Staley, J.P. The DExD/H-box ATPase Prp2p destabilizes and proofreads the catalytic RNA core of the spliceosome. *RNA* **20**, 282–294 (2014).
44. Konarska, M.M., Vilardell, J. & Query, C.C. Repositioning of the reaction intermediate within the catalytic center of the spliceosome. *Mol. Cell* **21**, 543–553 (2006).
45. Hilliker, A.K., Mefford, M.A. & Staley, J.P. U2 toggles iteratively between the stem IIa and stem IIc conformations to promote pre-mRNA splicing. *Genes Dev.* **21**, 821–834 (2007).
46. Branch, A.D., Levine, B.J. & Polaskova, J.A. An RNA tertiary structure of the hepatitis delta agent contains UV-sensitive bases U-712 and U-865 and can form in a bimolecular complex. *Nucleic Acids Res.* **23**, 491–499 (1995).
47. Pecoraro, V.L., Hermes, J.D. & Cleland, W.W. Stability constants of Mg^{2+} and Cd^{2+} complexes of adenine nucleotides and thionucleotides and rate constants for formation and dissociation of MgATP and MgADP. *Biochemistry* **23**, 5262–5271 (1984).

ONLINE METHODS

Yeast strains and plasmids. To test combinations of alleles in U2 and U6, we used strain yHM118, in which the endogenous genes encoding U2 and U6 were deleted and viability rescued with the *URA3*-marked plasmid pU2U6U[45]. To test, in addition, mutant versions of U4, we used strain yJPS628, containing pU2U6U4 (ref. 19). The *HIS3*-marked plasmid pJPS216 encodes U2 (ref. 48); the *TRP1*-marked plasmid pSX6 encodes U6 (ref. 15); and the *ADE2*-marked plasmid pJPS464 encodes U4 (ref. 19). Mutated U2, U6 and U4 plasmids, used for *in vivo* assays, were described previously[19] or generated for this study by QuikChange mutagenesis (Stratagene) and verified by sequencing. For *in vitro* transcription, mutant U6 templates were generated by QuikChange mutagenesis (Stratagene) from pJPS488, which encodes wild-type U6 downstream of a T7 promoter[49].

In vitro splicing was performed with extracts prepared from the following strains: yJPS1405 (*PRP19* with a C-terminal biotin tag[4]); yJPS1489 (*CWC2*-TAP, Open Biosystems[50]); yJPS1492 (*CWC25*-HA, same as ySCC25 (ref. 51)); yJPS1510 (*PRP19P*-HA, same as ySCC1 (ref. 36)).

Plasmid-shuffle growth assays. Variants of pJPS216 and pSX6 were cotransformed into yJPS328 and selected on plates lacking histidine and tryptophan. To test for interactions with U4, variants of pJPS216, pSX6 and pJPS464 were cotransformed and selected on plates lacking histidine, tryptophan and adenine. Duplicate colonies were grown in liquid medium lacking the appropriate nutrients to an OD_{600} of approximately 0.8 and then spotted onto medium containing 5-fluroorotic acid (5-FOA) to counter-select for the wild-type plasmid[52]. Cells were grown at 30 °C for 3–10 d for phenotypic analysis.

To test for a genetic interaction between *PRP16* and the U6 triplex, variants of pSX6 and wild-type pJPS216 were cotransformed into yHM187 (*prp16-302* (ref. 45)) or yHM118 (*PRP16*) and selected on plates lacking histidine and tryptophan. Duplicate colonies were grown in liquid medium lacking histidine and tryptophan to an OD_{600} of approximately 0.4 and then spotted onto medium containing 5-FOA to counter-select for the wild-type plasmid[52]. Cells were grown at 20 °C and photographed after 6 d.

The growth spots presented reflect two related growth parameters. First, the spots reflect colony size and consequently colony growth. Second, the spots reflect the number of colonies growing in the spot. Before equal numbers of cells were spotted onto 5-FOA to counter-select against cells that retained the wild-type *URA3*-marked plasmid, cultures were grown under selection for the mutated plasmids but not the wild-type plasmid. Phenotypically wild-type mutants passively lost the wild-type plasmid (~1–5% of cells/cell division) and consequently yielded a large fraction of cells that were viable on 5-FOA. By contrast, phenotypically sick or lethal mutants died in the culture if they passively lost the wild-type plasmid, so a large fraction of cells retained the wild-type *URA3*-marked plasmid and consequently died on 5-FOA, thus leading to spots with decreased colony density.

Copper growth assays. yJPS1035 (ref. 45) was first transformed with ACT1-CUP1 reporter variants on *LEU2*-marked plasmids (derived from pJPS1920 (ref. 45)) and then cotransformed with pJPS216 and pSX6 variants and selected on plates lacking histidine, tryptophan and leucine. Cotransformants were streaked onto medium lacking leucine and containing 5-FOA[52] and grown for 3 d at 30 °C. Colonies were then purified on minimal medium lacking leucine. Duplicate colonies were grown in liquid medium lacking leucine to an OD_{600} of approximately 0.2 and spotted on medium lacking leucine and containing various concentrations of copper sulfate. Cells were grown at 30 °C and photographed after 3 d.

Splicing extracts, U6 depletion and reconstitution, and *in vitro* splicing. Splicing extracts were prepared from yJPS1405 unless otherwise noted. Preparation of splicing extracts, *in vitro* splicing, U6 depletion and reconstitution, affinity purification via Prp19p and incubation of affinity-purified spliceosomes were performed essentially as described[4]. For cross-linking experiments, U6 was added back to a final concentration of 2–4 nM. *In vitro* splicing in extract was carried out for 25 min at 20 °C unless otherwise noted. Where noted, 20% of the standard splicing-extract volume was replaced with recombinant, dominant-negative Prp2p K252A, Prp16p K379A or Prp22p K512A in buffer D, at a final concentration of approximately 40–80 ng/μL.

Radiolabeled *ACT1* pre-mRNA was synthesized by *in vitro* transcription. Fluorescently labeled *UBC4* pre-mRNA was synthesized by splint-mediated ligation, essentially as described[53]. Radiolabeled 3′S-PS(R_P) and 3′O-PO pre-mRNAs were synthesized as described[4].

In **Figure 7b,c**, spliceosomes from extracts reconstituted with the indicated U6 variants were assembled on the 3′S-PS(R_P) substrate, affinity purified via Prp19p, and incubated in the absence of ATP in buffer PK (3% PEG, 60 mM KPO_4, pH 7.0) with 1 mM $MgCl_2$ or 1 mM $MnCl_2$ in the presence of various amounts of $CdCl_2$. In **Figure 7d**, spliceosomes from extracts reconstituted with the indicated U6 variants were assembled on the 3′S-PS(R_P) substrate, affinity purified via Prp19p, and incubated in the absence of ATP in buffer PK (pH 7.0) with 1 mM $MnCl_2$ in the presence of various amounts of $CdCl_2$.

Preparation of recombinant proteins. Recombinant Prp16p, Prp22p and Prp2p were expressed in *Escherichia coli* Rosetta2 DE3pLysS cells (Novagen), essentially as described[54]. Recombinant Prp2p was expressed in the presence of 2% ethanol at 17 °C for 17 h. All proteins were purified by Ni^{2+}-NTA affinity chromatography and subsequent glycerol gradient and were dialyzed against buffer D before use.

Synthesis of U6 snRNA for *in vitro* reconstitution. Synthetic U6, with modifications for cross-linking, was constructed by splint-mediated ligation with RNA oligonucleotides corresponding to the following U6 residues: 1–51, 52–79 and 80–112. Oligonucleotides 52–79 and 80–112 of U6 (containing U80 or ^{4S}U80) were purchased from Dharmacon, deprotected and used as supplied. U6 1–51 was generated from full-length, *in vitro*–transcribed U6 by DNAzyme-mediated cleavage after A51 with U6 A51 DNAzyme (5′-CTGATCATTCCGAGCCGG ACGACTGTATTGT-3′, a modified 8-17 DNAzyme[55]). For a typical cleavage reaction, 2–4 nmol of gel-purified, full-length, transcribed U6 was mixed with a 1.2-fold molar excess of U6 A51-Dzyme (IDT) in cleavage buffer (100 mM Tris-Cl, pH 7.4, and 50 mM NaCl) and then annealed by heating to 90 °C and subsequent cooling to room temperature for 25 min. After hybridization, cleavage was performed overnight at 37 °C in cleavage buffer supplemented with 10 mM $MgCl_2$. U6 1–51 product was gel purified, and the 3′-cyclic phosphate resulting from DNAzyme cleavage was removed by incubation with polynucleotide kinase (NEB) at 37 °C for 2–4 h. The U6 52–79 oligonucleotide was 5′ phosphorylated with [γ-^{32}P]ATP (PerkinElmer, 6,000 Ci/mmol) before ligation. Ligation of the three oligonucleotides and purification of ligated U6 was performed by splint-mediated ligation, as described[4].

Wild-type and mutant U6 used for the *in vitro* splicing experiments were synthesized by *in vitro* transcription according to standard procedures with templates derived from linearization of pJPS488 with DraI, as described[49].

UV cross-linking. For cross-linking[30], splicing reactions (20–40 μL) were transferred to a round-bottom 96-well plate (Fisher Scientific) on ice and irradiated with a UMP UV lamp (FBUVLS-80, Fisher Scientific) set at 365 nm and placed at approximately 4 cm from the bottom of the well so that light would shine perpendicularly on the plane of the sample. Irradiation was performed under an aluminum-foil tent at 4 °C for 90 min. After cross-linking, RNA was analyzed by 8% denaturing PAGE.

Analytical digestions. For nuclease P1 digestion, gel-purified X1 RNA (~3,000–10,000 c.p.m.) was incubated with nuclease P1 (1U/μL; US Biological) in a 4-μL reaction at 37 °C for 18–20 h. For alkaline hydrolysis, gel-purified RNA (~3,000–10,000 c.p.m.) was incubated with 20 mM NaOH at 90 °C for 3 h. After digestions, RNA was analyzed by 20% denaturing PAGE. For RNase H digestion of X3, gel-purified X3 RNA (~1,000 c.p.m.) was hybridized to 10 pmol of a DNA oligonucleotide complementary to U2 snRNA (nucleotides 35–62) or U4 snRNA (nucleotides 81–100) in buffer TEN (10 mM Tris, pH 7.4; 1 mM EDTA and 100 mM NaCl) in a 3-μL reaction volume on a thermal cycler. Cleavage was then performed by the addition of 1U RNase H (Fermentas) and incubation at 37 °C for 1 h.

NTC depletion and complementation. Splicing extracts were prepared from a strain containing Prp19p-HA (yJPS1510). For depletion, 200 μL of freshly prepared extract was incubated at 4 °C for 2 h with 150 μL of protein A–Sepharose

doi:10.1038/nsmb.2815

slurry conjugated to anti-HA antibodies (12CA5, University of Chicago Fitch Monoclonal Antibody Facility, 2 mg/mL of bead slurry)[56]. After centrifugation at 800*g* for 4 min, the supernatant was used as NTC-depleted extract.

For complementation, the NTC complex was isolated from yeast splicing extracts prepared from yJPS1510, as follows. The splicing extract was precipitated with 40% ammonium sulfate to obtain the 40P fraction, as described[57]. The 40P fraction (280 mg) was resuspended in 1 mL of buffer D supplemented with 60 mM potassium phosphate, pH 7.0 (buffer DK), and was incubated at 4 °C for 2 h with 200 µL slurry of protein A–Sepharose conjugated to anti-HA antibodies (12CA5, 2 mg/mL of bead slurry; cross-linked with DMP (Sigma)[58]. Beads were then washed three times at 4 °C with 6 mL of buffer DK supplemented with 0.01% NP-40 substitute (Fluka), brought to room temperature and washed with an additional 6 mL of the same buffer. The bound NTC was eluted with 300 µL of 0.6 mM HA peptide at room temperature with rotation for 30 min. The eluate was concentrated ten-fold with a Vivaspin-500 column (Sartorius), flash frozen and stored at –80 °C. Typically 1–2 µL of the concentrated NTC was used for complementation of a 10-µL splicing reaction.

Preparation of B^{act}, B*(prp16) and P complexes. To isolate B^{act} or B*(prp16) complex spliceosomes, splicing reactions (80 µL) were performed with *UBC4* pre-mRNA, labeled fluorescently with Cy3 at the seventh residue of the 3′ exon[53], and extracts from yJPS1492. The splicing reactions were supplemented with rPrp2p K252A, to accumulate B^{act}, or rPrp16p K379A, to accumulate B*(prp16), and were loaded on 11-mL 15–40% glycerol gradients in buffer G_{50} (20 mM HEPES, pH 7.9, 50 mM KCl and 0.5 mM EDTA). The gradients were centrifuged at 234,325*g* in a Beckman SW 41 rotor for 13 h. Fractions were collected by hand from the top of the gradient; RNA was extracted from the fractions and analyzed by denaturing PAGE. The splicing species were visualized by detection of the Cy3 label with a Typhoon Trio phosphorimager (Amersham Biosciences). The lariat intermediate generally peaked in fractions 16–20, so fractions 16–18 were collected to enrich for the B*(prp16) complex; the pre-mRNA generally peaked in fractions 18–22, so fractions 18–20 were collected to enrich for the B^{act} complex.

To isolate P-complex spliceosomes stalled after exon ligation, splicing reactions (80 µL) were performed with the fluorescently labeled *UBC4* pre-mRNA and supplemented with rPrp22p K512A with or without rPrp16p K379A. Reactions were run on glycerol gradients as above, and peak fractions for the lariat intermediate or excised intron were used for immunoprecipitation of spliceosomes associated with rPrp22p. The excised intron migrated with the lariat intermediate and peaked in fractions 16–20; fractions 17 or 18 were used for immunoprecipitation experiments.

Affinity pulldowns. For affinity purification of spliceosomes associated with biotinylated Prp19p, splicing reactions were diluted 1-fold to 2-fold in buffer D and incubated for 1–3 h at 4 °C with 0.1–0.2 volumes of streptavidin-agarose slurry (Thermo Scientific) prewashed twice with 25–50 volumes of IPP_{150} (10 mM Tris-HCl, pH 8, 150 mM NaCl, and 0.1% NP-40 substitute (Fluka)). Use of Streptavidin–agarose for immunoprecipitation of biotinylated Prp19 was verified previously[4]. After incubation, beads were washed at 4 °C twice with 50 volumes of IPP_{150}.

For immunoprecipitation of Prp16p-associated spliceosomes, peak glycerol-gradient fractions were diluted 1:1 in buffer DK_{150} (20 mM HEPES, pH 7.9, 150 mM KCl and 60 mM potassium phosphate, pH 7.0), and incubated for 1 h at 4 °C with 0.1–0.2 volumes of protein A–Sepharose slurry conjugated to affinity-purified anti-Prp16p antibodies (4–6 mg/mL of bead slurry; gift from C. Guthrie[38]). After immunoprecipitation, beads were washed at 4 °C twice with 50 volumes of buffer DK_{150} supplemented with 0.01% NP-40 substitute.

For immunoprecipitation of Prp22p-associated spliceosomes, peak glycerol-gradient fractions were diluted 1:1 in buffer DK_{150} and incubated for 1 h at 4 °C with 0.1–0.2 volumes of protein A–Sepharose slurry conjugated to affinity-purified anti-Prp22p antibodies (1.5 mg/mL of bead slurry; gift from B. Schwer[40]). After immunoprecipitation, beads were washed at 4 °C twice with 50 volumes of buffer NET-2 (50 mM Tris-HCl, pH 7.4, 150 mM NaCl, and 0.05% NP-40 substitute).

Cwc2 depletion and complementation. Splicing extracts prepared from yJPS1489 (Cwc2-TAP) were depleted of Cwc2p essentially as described[2].

For expression of rCwc2p, the *CWC2* sequence was amplified from a plasmid containing the *CWC2* ORF (bJPS2509, Open Biosystems) and cloned into pET15b (bJPS581) with the NdeI and BamHI cloning sites to give bJPS2621. The cloned plasmid was verified by sequencing. Expression of His_6-rCwc2p was performed in *E. coli* Rosetta2 DE3pLysS cells. Cells were grown at 37 °C to OD_{600} ~0.8, and expression was induced with 0.5 mM IPTG at 30 °C for 3 h. Cells were lysed with a French press, and His_6-rCwc2p was purified by Ni^{2+}-NTA affinity chromatography, but binding and washing were performed by gravity flow. After elution from the Ni^{2+}-NTA resin, the protein was further purified by glycerol-gradient centrifugation to more than 95% purity (as estimated by Coomassie blue staining) and dialyzed against buffer D. For complementation of Cwc2p-depleted extracts, rCwc2p was added back at a final concentration of 2–4 µM.

Original images of gels and autoradiographs used in this study can be found in **Supplementary Figure 8**.

48. Shuster, E.O. & Guthrie, C. Two conserved domains of yeast U2 snRNA are separated by 945 nonessential nucleotides. *Cell* **55**, 41–48 (1988).
49. Fabrizio, P., McPheeters, D.S. & Abelson, J. *In vitro* assembly of yeast U6 snRNP: a functional assay. *Genes Dev.* **3**, 2137–2150 (1989).
50. Ghaemmaghami, S. *et al.* Global analysis of protein expression in yeast. *Nature* **425**, 737–741 (2003).
51. Chiu, Y.-F. *et al.* Cwc25 is a novel splicing factor required after Prp2 and Yju2 to facilitate the first catalytic reaction. *Mol. Cell. Biol.* **29**, 5671–5678 (2009).
52. Sikorski, R.S. & Boeke, J.D. *In vitro* mutagenesis and plasmid shuffling: from cloned gene to mutant yeast. *Methods Enzymol.* **194**, 302–318 (1991).
53. Abelson, J. *et al.* Conformational dynamics of single pre-mRNA molecules during in vitro splicing. *Nat. Struct. Mol. Biol.* **17**, 504–512 (2010).
54. Schneider, S., Hotz, H. & Schwer, B. Characterization of dominant-negative mutants of the DEAH-box splicing factors Prp22 and Prp16. *J. Biol. Chem.* **277**, 15452–15458 (2002).
55. Silverman, S.K. *In vitro* selection, characterization, and application of deoxyribozymes that cleave RNA. *Nucleic Acids Res.* **33**, 6151–6163 (2005).
56. Tarn, W.Y., Lee, K.R. & Cheng, S.C. Yeast precursor mRNA processing protein PRP19 associates with the spliceosome concomitant with or just after dissociation of U4 small nuclear RNA. *Proc. Natl. Acad. Sci. USA* **90**, 10821–10825 (1993).
57. Cheng, S.C., Newman, A.N., Lin, R.J., McFarland, G.D. & Abelson, J.N. Preparation and fractionation of yeast splicing extract. *Methods Enzymol.* **181**, 89–96 (1990).
58. Tarn, W.Y. *et al.* Functional association of essential splicing factor(s) with PRP19 in a protein complex. *EMBO J.* **13**, 2421–2431 (1994).